Energy Deposition and Shock Wave Evolution from Laser-Generated Plasma Expansions

J.J. MacFarlane, G.A. Moses, R.R. Peterson

May 1987

UWFDM-723

Phys. Fluids B1 (1989) 635.

FUSION TECHNOLOGY INSTITUTE

UNIVERSITY OF WISCONSIN

MADISON WISCONSIN

Energy Deposition and Shock Wave Evolution from Laser-Generated Plasma Expansions

J.J. MacFarlane, G.A. Moses, R.R. Peterson

Fusion Technology Institute
University of Wisconsin
1500 Engineering Drive
Madison, WI 53706

http://fti.neep.wisc.edu

May 1987

UWFDM-723

Phys. Fluids B1 (1989) 635.

ENERGY DEPOSITION AND SHOCK WAVE EVOLUTION FROM LASER-GENERATED PLASMA EXPANSIONS

J.J. MacFarlane

G.A. Moses

R.R. Peterson

Fusion Technology Institute
1500 Johnson Drive
University of Wisconsin-Madison
Madison, Wisconsin 53706

May 1987

UWFDM-723

I. Introduction

The formation and evolution of shock waves resulting from laser-generated plasma expansions have been studied extensively in a series of recent experiments.[1-7] Such studies provide valuable data for testing theoretical approaches used to model physical processes occurring in laboratory and astrophysical plasmas. As an example, in proposed inertial confinement fusion (ICF) test facilities and reactors,[8,9] deuterium-tritium fuel pellets are expected to release up to several hundred megajoules of energy in the form of x-rays, neutrons, and ionized debris. If the explosion occurs in a high density background gas, the debris ions and soft x-rays will be absorbed very close to the pellet, substantially heating and ionizing the surrounding gas. The resulting pressure increase causes the formation of a blast wave that is well-described analytically by strong shock theory.[10] However, if the density of the background gas is lowered to the point that the collisional mean free path of the expanding debris becomes large, the pellet energy is deposited over a much larger volume. Consequently, the energy release cannot be treated as an instantaneous point explosion, and strong shock theory is not applicable. In this case, a more detailed calculation is required to accurately determine the hydrodynamic properties of the blast wave. Also, radiation losses can become important and may lead to less energy being transformed into hydrodynamic energy. This can result in a substantially weaker blast wave. Finally, the time interval over which energy is deposited at the wall of the target chamber decreases as the gas pressure decreases, producing a greater thermal stress on the wall. Thus, the degree to which energy is absorbed by the background gas can play an large role in determining which physical processes will be important inside ICF target chambers.

In this paper, we present the results from radiation-hydrodynamic calculations of an ionized plasma expanding into a background gas of varying density. The results are compared with experimental data recently obtained at the Naval Research Laboratory (NRL).[3,4,6] In the NRL experiments we have simulated, a solid planar aluminum target was illuminated by an intense laser pulse ($\sim 10^{12}$ W/cm^2 with pulse width $\sim$ 5 ns), producing an explosion of highly charged Al ions with velocities $\sim 5 \times 10^7$ cm/s. The Al ions transfer energy and momentum (via collisions) to a surrounding nitrogen gas, producing significant ionization, and heating the gas to $\sim 10^2$ eV. Also, the Al ions, which are fully ionized as they leave the target,[11] undergo charge-exchange and electron-capture reactions as they speed through the background gas. Thus, the ionization state of the Al ions decreases as they travel through the gas. The ambient pressure of the background N_2 gas was varied from $\sim 10^{-2}$ to 10^1 torr (room temperature values). The location of the shock front as it evolved was monitored using both dark-field shadowgraphy and framing photography.[2,6] In addition, spectroscopic observations were made to estimate the temperature, density, and charge state of the plasma.[3]

The background pressures in our calculations cover a range that varies from the high density, "collisional" regime to the low density, "collisionless" regime. That is, for background gas pressures $\gtrsim$ 1 torr, essentially all of the kinetic energy of the debris ions is lost in collisions with background gas particles that occur within a very small volume near the target. At gas pressures $\lesssim$ 0.1 torr, a large fraction of the debris ions will stream through the background gas while depositing very little of their energy. The purpose of this study is to gain a better understanding of the interaction, or "coupling", between the exploding plasma and the background medium in this

transition region. In particular, we wish to determine whether classical collision theory can adequately explain the experimental data, or whether other effects, such as plasma instabilities, must be invoked.

In Section II, we outline the theoretical models and assumptions used in our calculations. In Section III, the results of our computations and comparisons with experimental data are presented. Here, we will first describe results in which radiation losses are neglected (i.e., radiation transport is not included in the energy equations). Then we will show how radiation transport affects the properties of blast waves. Finally, we summarize our results and conclusions in Section IV.

II. Theoretical Models and Assumptions

We have performed the calculations discussed in this paper with a one-dimensional radiation-hydrodynamics code called CONRAD.[12] A detailed description of the radiation and hydrodynamic equations has been provided elsewhere,[13] and only a brief outline will be presented below. Here, we shall emphasize the procedure used to calculate the transfer of energy from the target debris ions to the background gas.

A) Ion Energy Deposition Model

We assume in our calculations that the only energy source (other than the ambient thermal energy of the background gas) is the kinetic energy of the debris ions. The velocity distribution of the ions emitted from the target is well known from experiments performed with essentially no background gas surrounding the target. It is more difficult, however, to determine the appropriate debris mass to use in our 1-D spherical calculations because of the non-isotropic nature of the plasma expansion in the experiments. Measurements

obtained from experiments in which approximately 100 J of laser energy was focused onto a planar target[4] indicate that roughly 50 J of debris kinetic energy (0.4 μg of ions with $\langle v_{ion} \rangle \sim$ 450-500 km/s) expands into the hemisphere facing the incoming laser beam. Roughly half of that was contained in a cone of solid angle $\sim \pi/2$, and whose axis of symmetry lies perpendicular to the target (along the laser axis). Since most measurements of the shock properties were made in the solid angle where the debris concentration was highest, an equivalent value to use for the Al kinetic energy expanding into 4π steradians in our simulations is ~ 150-200 J. That is, we simulate the NRL experiments using an isotropic spherical expansion of Al ions having a kinetic energy of ~ 12-16 J/steradian.

In assuming the debris ion kinetic energy is the sole energy source, we have neglected the energy emitted from the target in the form of x-rays. These x-rays partially ionize (0.2%) and heat the background gas to ~ 1-2 eV [5] before the target ions arrive. Ripin et al.[2] estimate that ~ 90% of the energy absorbed by the target is converted to debris energy. Thus, we can expect the target x-ray energy emitted to be $\lesssim$ 10% of the absorbed energy. Because the uncertainties in estimating the debris ion kinetic energy are much larger, we have chosen to neglect the effect of the target x-rays.

A time- and energy-dependent model is used to compute the debris ion energy deposition. The ions are assumed to explode isotropically from the target area with a constant flux over a period approximately equal to the laser pulse width (~ 5 ns). Their velocity spectrum is divided into 10 different energy groups, and the time interval over which the ions are emitted is divided into 100 time bins. The Al ions transfer energy to the background gas through collisions at a rate determined by the ion stopping cross-sections.

The energy and location of each ion group is tracked until the ion velocities eventually fall below the thermal velocity of the gas, or until they escape the computational grid.

The ion stopping cross-sections are calculated using a model similar to that described by Melhorn.[14] The debris ions interact with the background gas via ion-neutral, ion-ion, and ion-electron collisions. Other processes, such as plasma instabilities, are not included. The stopping cross-section is defined to be the increment of energy dE lost by a "projectile" ion (here, an Al ion) as it travels a distance dx through a material of atomic number density N. Mathematically, the stopping cross-section can be written as:

$$S = \frac{1}{N}\frac{dE}{dx} = S_n + S_{be} + S_{fe} + S_{ii} \quad . \tag{1}$$

S_n and S_{be} are the contributions from elastic nuclear scattering and inelastic scattering from bound electrons, respectively. These arise from ion-neutral collisions and are therefore important only at lower temperatures. S_{fe} represents the contribution from collisions between the debris ions and free electrons, and becomes important at temperatures $\gtrsim$ 1 eV. The ion-ion term, S_{ii}, contributes only at very high temperatures ($\gtrsim 10^3$ eV), and can be ignored for the problems discussed here.

When the debris ion velocities are small compared to the orbital "velocities" of the bound electrons ($\sim v_o \equiv$ velocity of an electron in the first Bohr orbit of hydrogen $\sim 2.2 \times 10^8$ cm/s), the stopping cross-sections for ion-neutral collision are calculated using the Lindhard-Scharff model,[15] which is based on Thomas-Fermi theory.[16] At higher ion velocities, these cross-sections are calculated using the Bethe model.[14] Comparisons between the

theoretical stopping cross-sections and experimental data are shown in Figs. 1 and 2. The cross-sections for protons (Fig. 1) and aluminum ions (Fig. 2) traveling through nitrogen at room temperature are plotted as a function of the ion kinetic energy. The theoretical values are indicated by the solid line in each figure. Data taken from the tables of Northcliffe and Schilling[17] are indicated by the dashed lines. This data is based on a combination of experimental data and theoretical models. Also shown in Fig. 1 is a dotted curve which is a fit to experimental data.[18]

Figure 1 shows the theoretical stopping cross-sections for protons are in excellent agreement with the experimental data over the entire energy range. The Northcliffe and Schilling data also agrees with the experimental data for ions with kinetic energies $\gtrsim$ 200 keV, but are up to a factor of 2 too low at lower energies. In this plot, the total cross-sections are dominated by the inelastic scattering term S_{be}. In Fig. 2, elastic collisions (S_n) make the largest contribution for kinetic energies below 100 keV. Here, the theoretical values for Al agree well with the Northcliffe and Schilling data. Unfortunately, experimental data for relatively heavy projectiles is sparse at energies relevant to the NRL experiments ($< 10^2$ keV). Even so, Ormrod et al.[19] have shown that the Lindhard-Scharff model is in general agreement with experimental data (within a factor of 2) for a wide variety of projectiles and stopping media. Consequently, we feel the low temperature contributions to the theoretical stopping cross-sections should be fairly reliable.

At higher temperatures, the background gas becomes ionized and the stopping powers become dominated by electron-ion collisions. The free electron stopping cross-section is proportional to the square of the charge state of

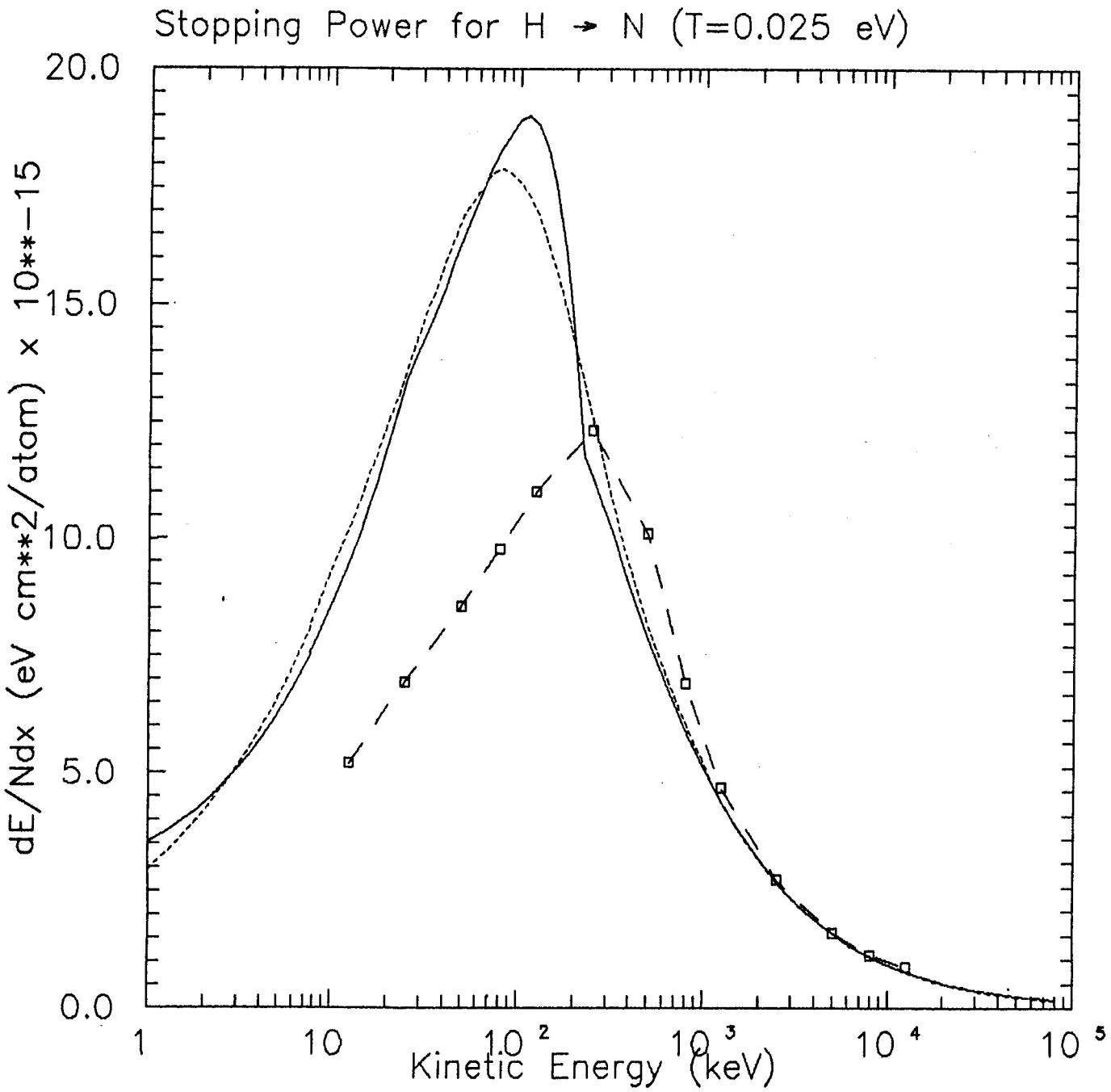

Fig. 1. Stopping cross-sections for protons in nitrogen at room temperature as a function of proton kinetic energy. Results are shown for theoretical calculations (solid curve), fit to experimental data (dotted curve), and Northcliffe and Schilling tables (dashed curve).

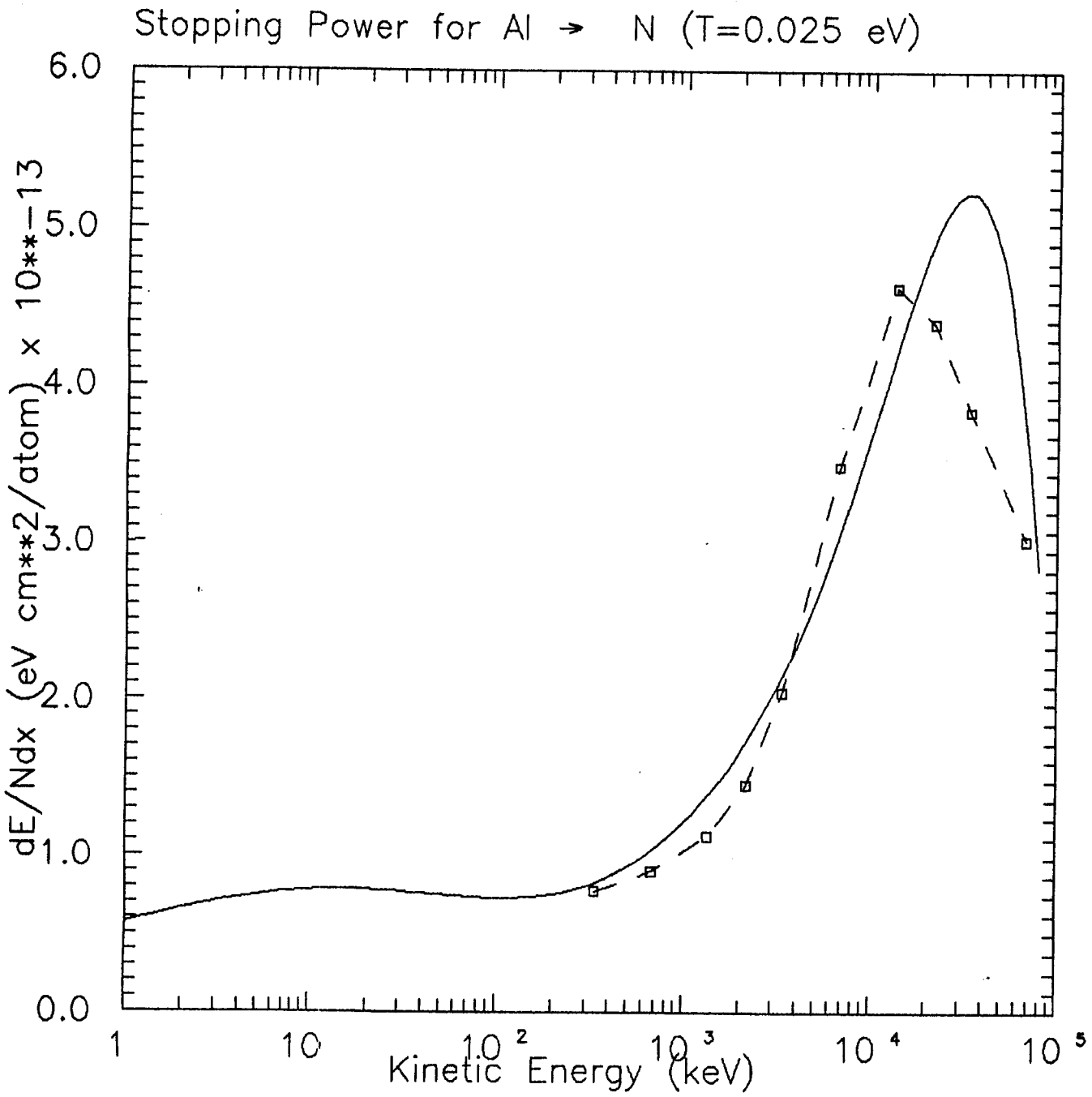

Fig. 2. Stopping cross-sections for aluminum in nitrogen at room temperature as a function of aluminum kinetic energy. Results are shown for theoretical calculations (solid curve) and Northcliffe and Schilling tables (dashed curve).

the projectile ion Z_1^* ($S_{fe} \propto (Z_1^*)^2$).[19] Figure 3 shows the theoretical total stopping cross-sections for Al ions traveling through a partially ionized nitrogen plasma. The temperature is 10 eV and the average charge state of the nitrogen is assumed to be 2. The three curves were calculated for three different values of the projectile charge states: Al^{7+} (top curve), Al^{4+}, and Al^{1+} (bottom curve). At an energy typically observed in the NRL experiments, say ~ 30 keV, the ion stopping power for Al^{7+} is predicted to be roughly 10 times higher than that for singly ionized aluminum. The reason for this is the larger Coulomb field originating from the more highly charged ion results in greater momentum transfer to the electron.

The strong dependence of the total stopping cross-section on the projectile charge indicates the importance of knowing the charge state of the Al ions as they evolve in time. This of course requires calculating the cross-sections for charge-exchange and electron-capture reactions for the various ionization states of Al as a function of velocity. Because of the complexity involved in calculating these cross-sections, we have used an "average" charge for the Al ions, which in effect becomes an adjustable parameter. The sensitivity of the results to this average charge is addressed in Section III.

B) Hydrodynamic and Radiation Models

As the debris ions collide with and heat the background gas, energy is transported away from the target by radiation, electron conduction, and hydrodynamic motion. The mass, momentum, and energy conservation equations are solved using single-fluid Lagrangian hydrodynamics. Equation of state tables are computed assuming local thermodynamic equilibrium (LTE), with the ionization states calculated using the Saha equation at high densities and low

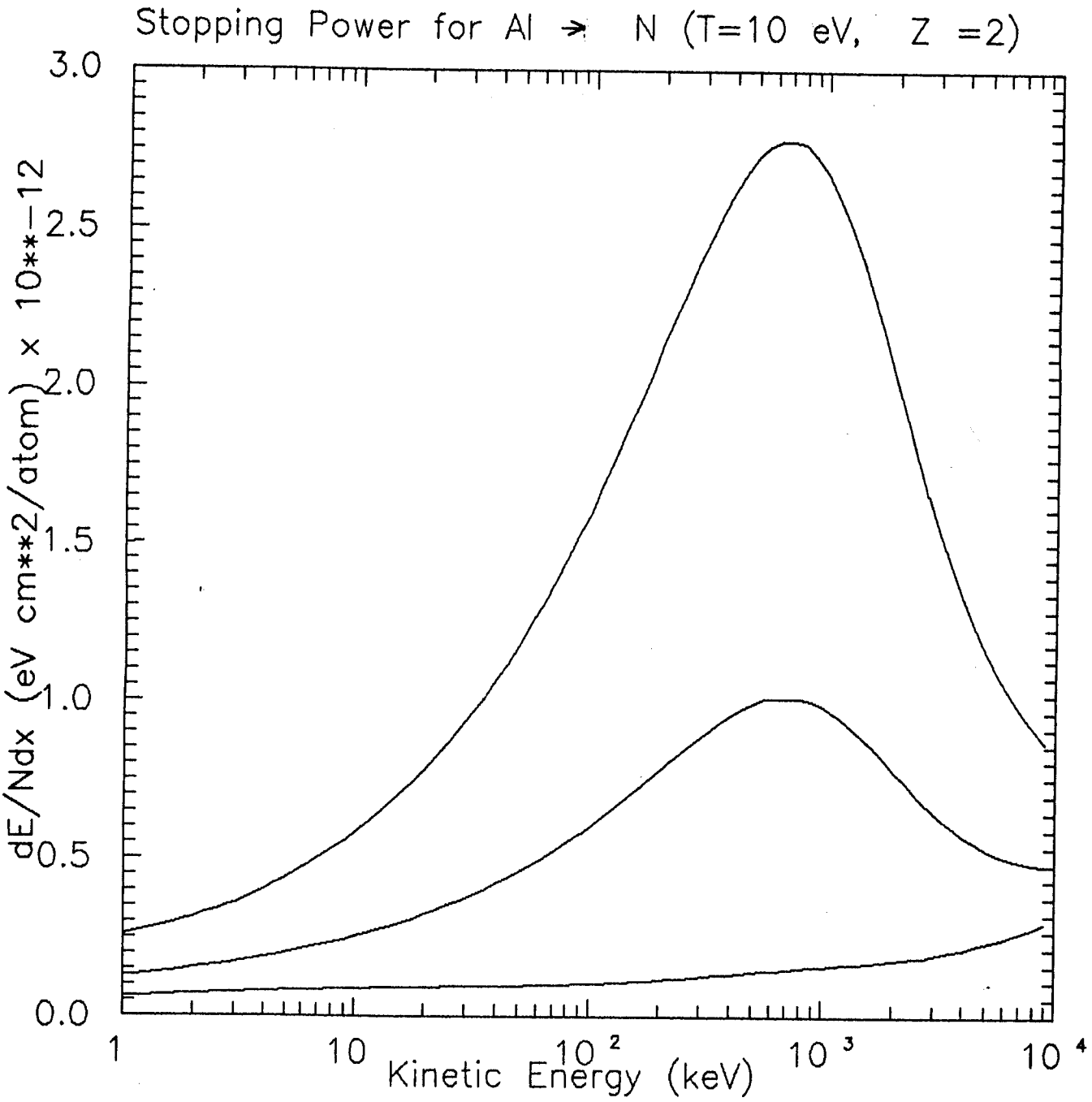

Fig. 3. Calculated stopping cross-sections for aluminum in nitrogen at T = 10 eV as a function of aluminum kinetic energy. Curves correspond to Al charge states of 7 (top), 4 (middle), and 1 (bottom).

temperatures, and the coronal equilibrium model elsewhere. The ions and electrons are assumed to be in equilibrium, and thus have the same temperature. A detailed description of the computer code used to generate the equation of state data (called MIXERG) is given elsewhere.[21]

Multigroup radiation transport equations are solved using the flux-limited diffusion approximation.[22] This approach, which assumes the photon mean free paths are small compared to the characteristic lengths in the problem, is not always reasonable for the conditions that occur in the NRL experiments. Therefore, we expect the radiation model may produce somewhat inaccurate, though not physically unreasonable, results. Radiation is transported using 20 frequency groups. The opacity tables used were calculated with MIXERG.

Although no experimental data exists that can be used to assess the accuracy of the opacities and equation of state at high temperatures, comparison with other theoretical results can give an indication of the uncertainty in these values. Comparisons between the MIXERG data and the Astrophysical Opacities Library (AOL) at Los Alamos[23] indicate that the MIXERG opacities are somewhat lower (about an order of magnitude or so) than the AOL values at photon energies $\lesssim$ 10 eV. This may be caused by the somewhat simple model used by MIXERG to calculate the contributions from bound-bound transitions. On the other hand, the degree of ionization predicted at high temperatures ($\gtrsim$ 20 eV) is significantly higher in the AOL tables for nitrogen. In this case, it appears the AOL calculation may be relying on the Saha model at all temperatures, and may therefore be inaccurate. In any case, we will show below that radiation transport can significantly affect the results of our simulations.

III. Results

Next, we present the results of our calculations and compare them with experimental data. We have performed simulations in which Al ions expand isotropically into a nitrogen background gas. The initial gas pressures selected for our calculations range from 0.025 to 5.0 torr. The velocity distribution for the Al ions was chosen to approximate experimental time-of-flight data,[4] and the total kinetic energy of the ions was varied by adjusting the total mass of the exploding Al. We assumed an average charge state of 4 for the Al ions, unless otherwise indicated.

In the first part of this section, we will describe the results from simulations in which radiative transfer is neglected. In these problems, energy is transported away from the target by electron conduction and hydrodynamic motion. Results from calculations in which the diffusion approximation is used to model radiation transport will be discussed in the second part of this section. We have performed calculations with and without radiation in order to assess the importance of radiation energy losses, and also to test the validity of using the radiation diffusion approach under the conditions that existed in the NRL experiments.

A) Hydrodynamic Calculations

Some typical results from our calculations are shown in Figs. 4(a) through 4(e). Plotted as a function of distance from the target are the plasma temperature, pressure, mass density, electron density, and fluid velocity. The different curves in each figure represent simulation times ranging from ~ 40 ns to ~ 250 ns (the shock moves from left to right in these figures). The total debris ion kinetic energy used in this calculation was 70

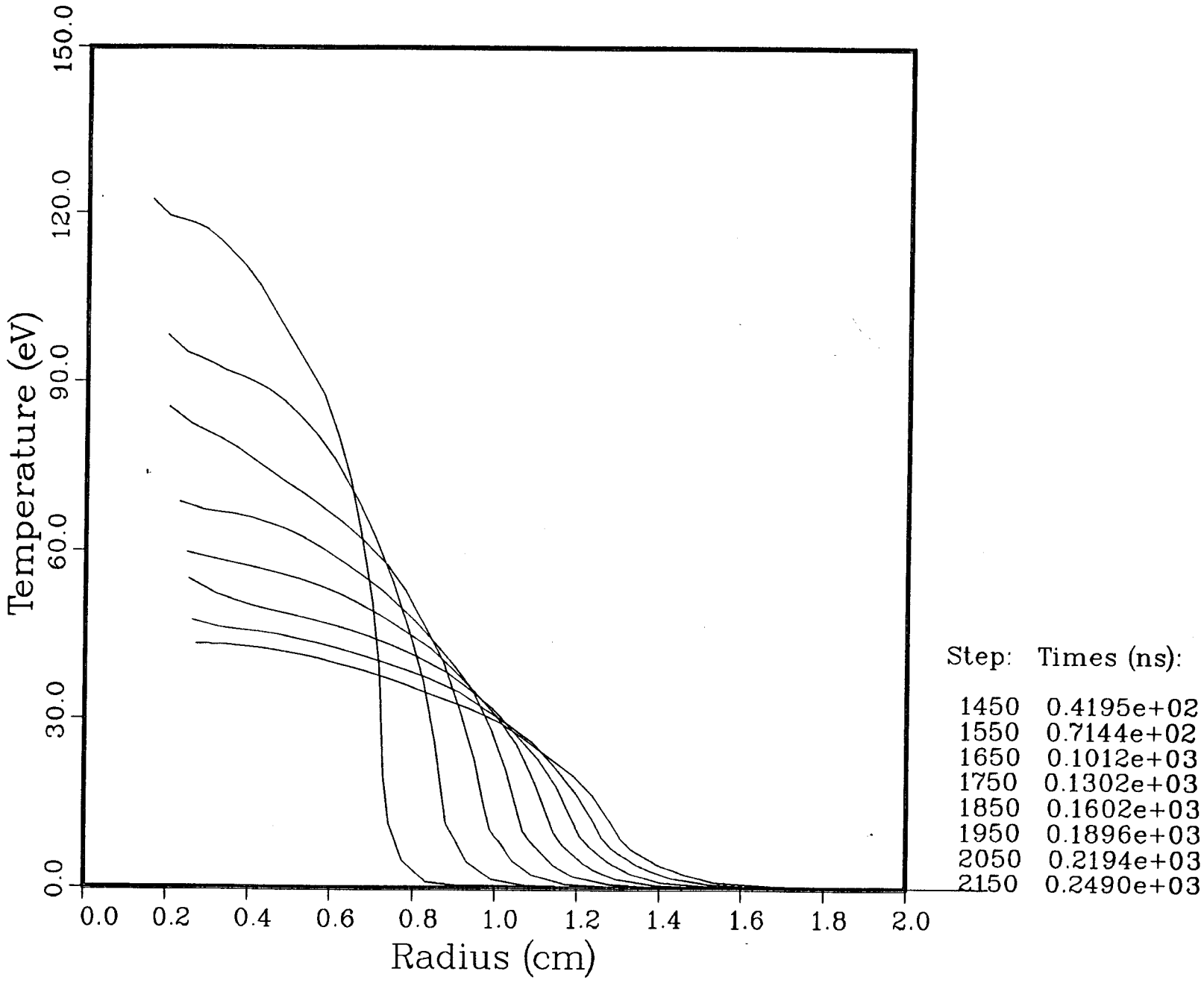

Fig. 4(a). Calculated plasma temperature as a function of radius at 8 different simulation times. Total Al kinetic energy was 70 J, and radiation effects were not included.

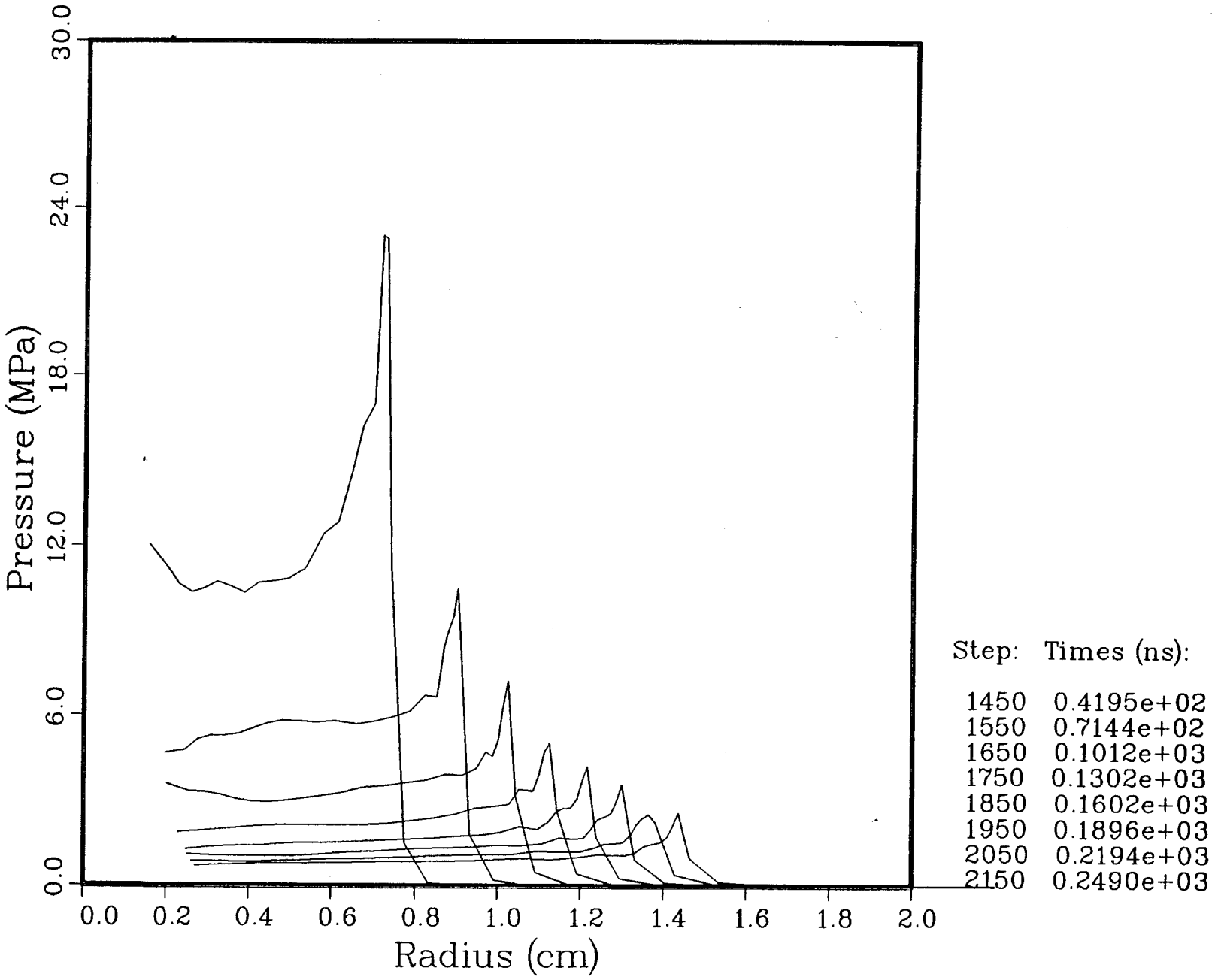

Fig. 4(b). Plasma pressure vs. radius (same calculation as Fig. 4(a)).

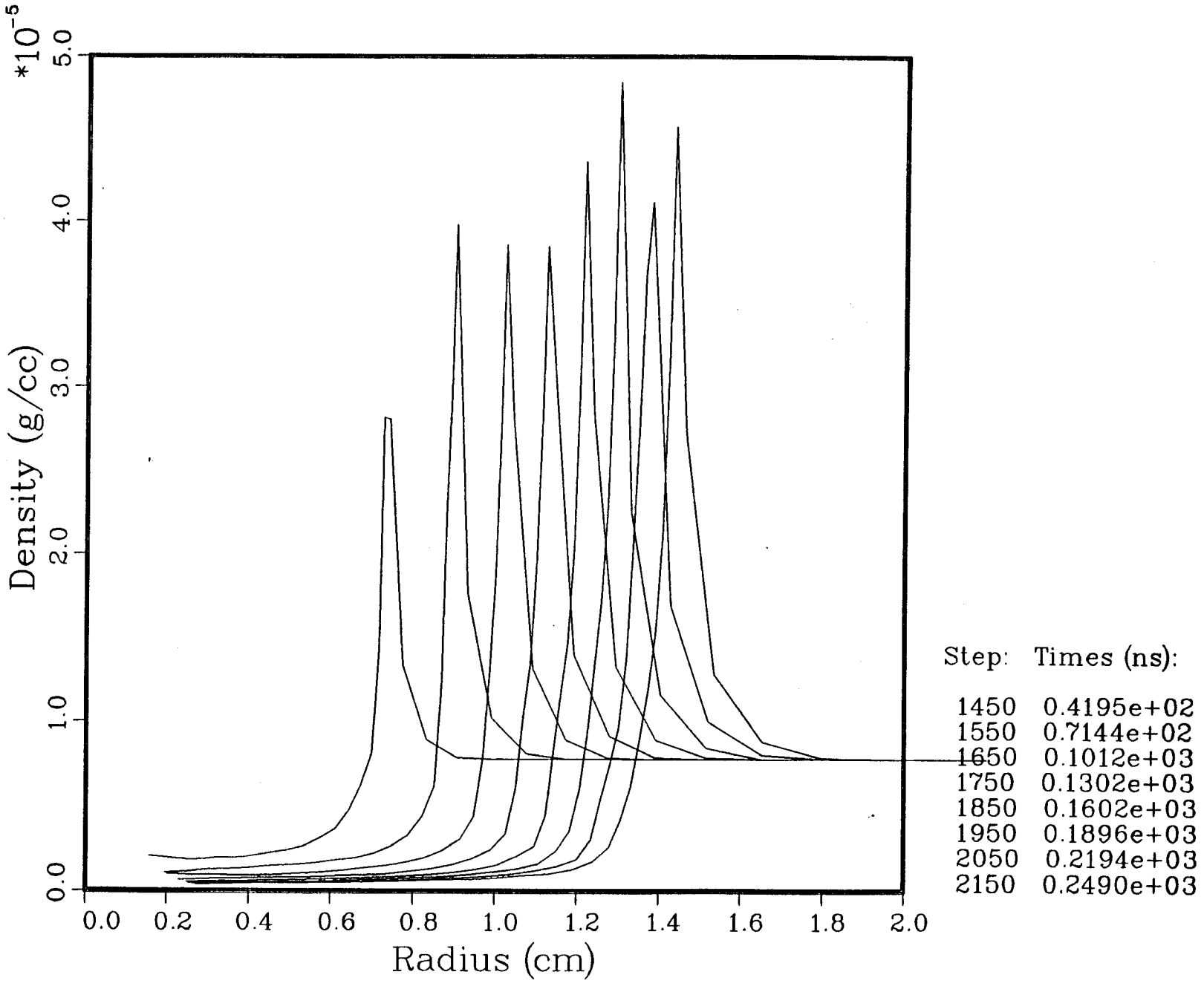

Fig. 4(c). Mass density vs. radius (same calculation as Fig. 4(a)).

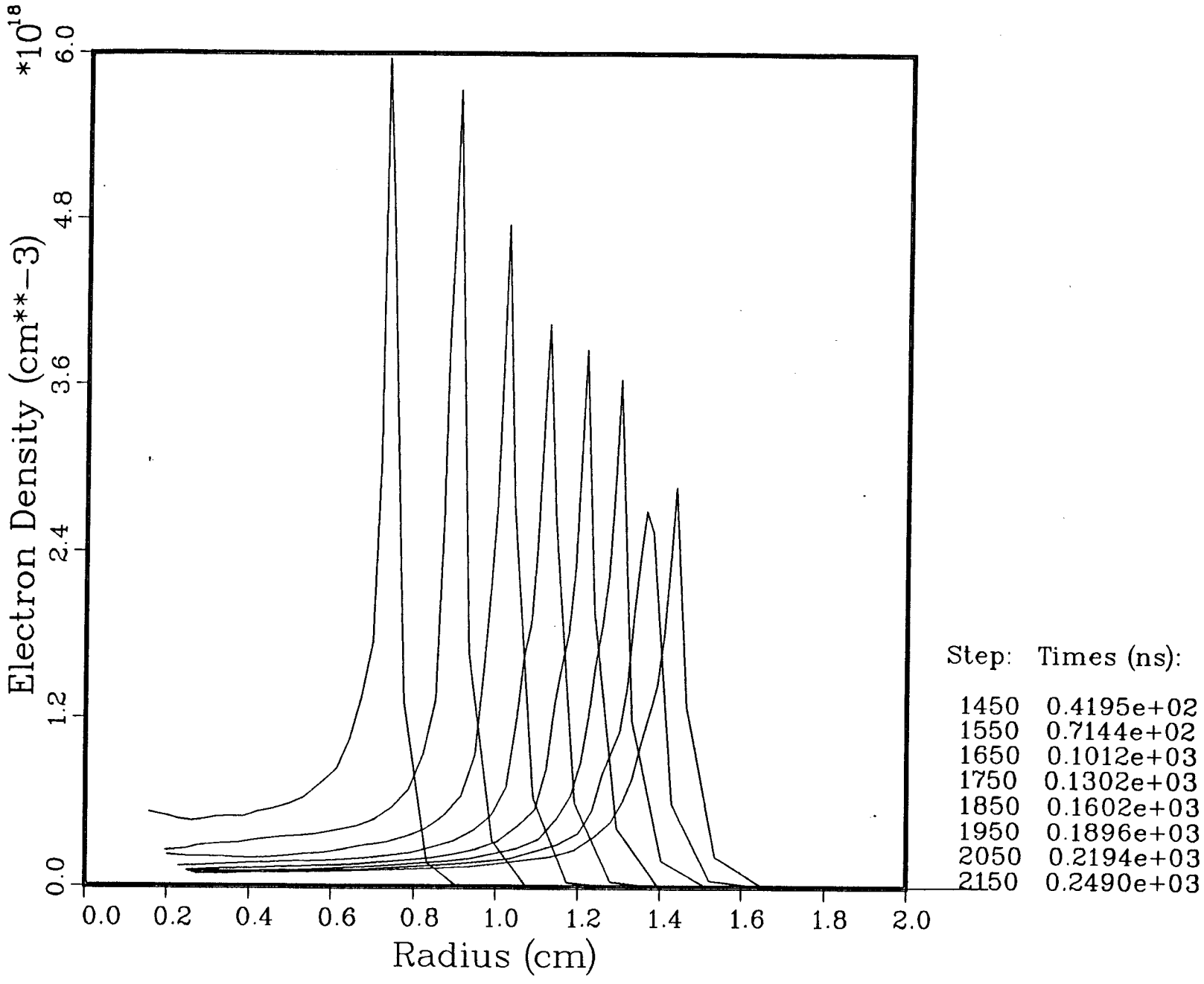

Fig. 4(d). Electron density vs. radius (same calculation as Fig. 4(a)).

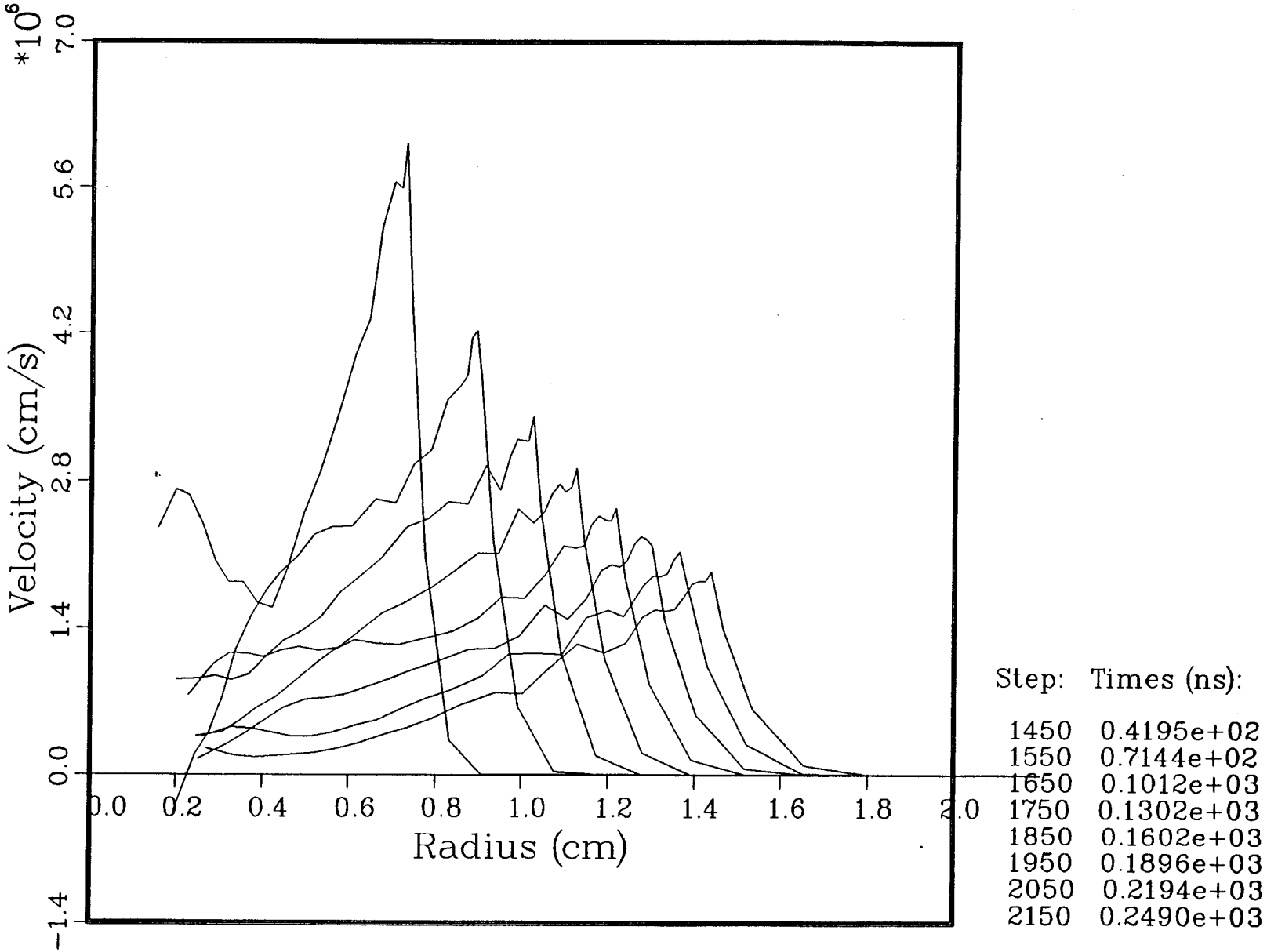

Fig. 4(e). Fluid velocity vs. radius (same calculation as Fig. 4(a)).

J, and the initial gas pressure was 5 torr. Radiation transport was not included in this calculation.

The most noticeable feature in Figs. 4(b) through 4(e) is the presence of a strong shock front. The front travels radially outward with a velocity ~ a few x 10^7 cm/s at early times, and slows as it sweeps up mass from the background gas. The shock front is quite clearly defined in simulations with this initial gas pressure, with the peak values for the pressure, fluid velocity, mass density, and electron density all occurring at about the same radius. Behind the shock front is a hot, low density microfireball, where the temperature distribution is roughly isothermal near the center. At the times shown, the temperatures are high enough to substantially ionize the gas in the fireball region.

We can compare the results from this calculation with observations from experimental shots in which 25 J of laser energy was focused onto an Al foil target.[3] In this experiment, the initial gas pressure surrounding the target was 5 torr, and the gas was composed of 90% N_2 and 10% H_2. From spectroscopic data, McLean et al.[3] have determined that the shock front reaches a radius of 1 cm (perpendicular to the target) at ~ 100 ns. Also, they have estimated the peak electron density at that point to be roughly 5 x 10^{18} cm^{-3}, and placed an upper limit of ~ 14 eV for the electron temperature. The uncertainty in the temperature, however, is rather large because of the assumption that N^{2+} would be the highest observable ionization state. These observations are reasonably consistent with the results plotted in Fig. 4. Our calculations predict a shock arrival time at 1 cm of 95 ns, a peak electron density at 1 cm of 4.7 x 10^{18} cm^{-3}, and a peak temperature at 1 cm of 30 eV. The differences between the calculated and experimental temperatures may be due to either neglecting

radiation losses in our calculations (discussed in more detail in Section III.B), or simply because of the large uncertainties in the experimental determination. But overall, the 25 J laser energy experiments are well-described by our 1-D hydrodynamic simulations using a total debris ion kinetic energy of 70 J (or ~ 5.6 J/steradian).

It is somewhat surprising that the debris ion kinetic energy required by our calculations to predict the experimentally observed shock arrival time at 1 cm is so large. In Section II.A, we estimated that a debris ion energy (E_{ion}) of ~ 150-200 J expanding into 4π steradians in our calculations should produce the same ion concentration that was observed in the experiments using 100 J of laser energy (E_{laser}) on target. That is, the ratio of the debris ion energy used in our simulations to the experimental laser energy is E_{ion}/E_{laser} ~ 1.5-2.0. However, to predict the shock arrival time observed in the experiments using 25 J of laser energy, our calculations require E_{ion}/E_{laser} ~ 70 J/25 J ~ 2.8. This larger ratio is likely caused by differences in the debris expansion characteristics between the 25 J and 100 J laser energy experiments. For example, the anisotropy in the plasma expansion may have been more pronounced in the 25 J experiments, or perhaps the velocity spectra of the target ions were significantly different. These effects could result from differences in the laser spot size focused on the target, the pulse duration, or the laser beam intensity.[1,25]

It is also of interest to track the evolution of the shock front as it propagates away from the target area. This is because the shock velocity provides information about how much energy from the debris ions has been "coupled" into the background gas. For instance, overestimating the ion stopping cross-sections will result in shorter mean free paths for the Al ions,

and energy will be absorbed by the background gas closer to the target. And if the ion stopping range is comparable to or larger than the shock radius, the resulting shock radius will be too large. Comparisons between our calculated shock radii and experimental observations are shown in Fig. 5 as a function of time. In these calculations, the total debris ion energy was 150 J ($\sim$ 12 J/steradian). The solid curves represent the calculated radii for 4 different initial gas pressures: 0.1 (at top), 0.3, 1.5, and 5 torr. The open symbols in each plot represent the shock positions observed in NRL experiments in which 100 J of laser energy was focused onto the Al target. The straight dashed line originating from the origin represents the initial velocity of the debris ions ($\sim 5 \times 10^7$ cm/s). The experimental data were obtained using framing photography of the visible emission fronts.[6] Because the emission is a strong function of the electron density,[6] we have defined the location of the shock front in our simulations to be the radius at which the electron density was a maximum.

Figure 5 shows that the calculated shock radii are in reasonable agreement with the experimental data at all pressures. The calculated shock radii for the 0.1 and 0.3 torr cases are slightly greater than the experimental values, while the radii for the 1.5 torr case agree quite well with the data. In the 5 torr problem, the computed radius agrees with the NRL data at early times ($\lesssim$ 100 ns), but predicts a somewhat larger radius at later times. It is worth noting that the calculated curve at 5 torr has a trajectory that is quite similar to that predicted by strong shock theory ($r \propto t^{2/5}$).[10] Although there is some "scatter" in the NRL data, the experimental shock velocities are noticeably smaller than the calculated velocities at times $\gtrsim$ 100 ns. Thus, it

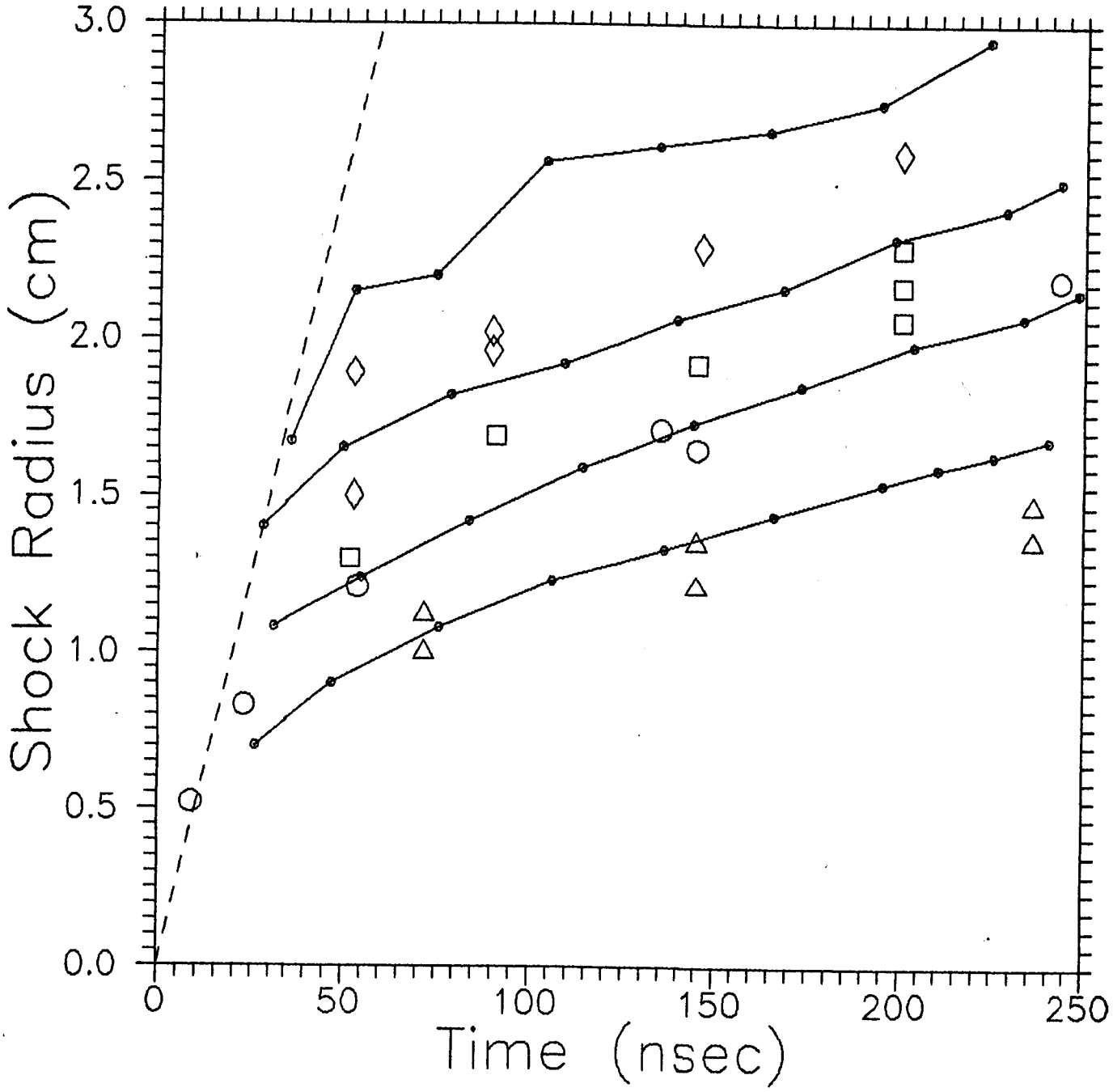

Fig. 5. Shock front radius vs. time. Solid curves represent calculated values. Radiation effects were not included. Experimental data as shown for ambient gas pressures of 0.1 torr (diamonds), 0.3 torr (squares), 1.5 torr (circles), and 5.0 torr (triangles).

appears that the part of the shock front observed in the NRL experiment, which is perpendicular to the target and along the laser axis, is losing a significant amount of energy at these times. One explanation for this is a significant amount of radiant energy may be escaping from behind the shock front in the NRL experiments. Another possibility is that energy that was preferentially deposited along the laser axis (due to the anisotropic debris ion flux) may be diffusing away from this axis. In this case, the shock front would become more spherical as the energy is redistributed away from the laser axis.

The sensitivity of our results to the uncertainties in the charge states of the Al ions is illustrated in Fig. 6. As discussed in Section II.A, we can adjust the energy deposition range of the Al ions by modifying the average charge state used in calculating the free electron stopping cross-sections. Figure 6 compares the results of calculations using different values for the Al charge state for both the 0.1 and 5 torr problems. The solid curves represent the shock radii computed using an ionization state of Al^{4+}, and the dashed curves represent similar results for Al^{2+}. The open symbols represent the experimental values. In these calculations, the debris ion kinetic energy was again 150 J, and radiation transport was neglected. The shock radius is seen to be quite sensitive to the charge state of the debris ions at 0.1 torr. An ionization state of 3 would produce good agreement with the experimental data. At higher pressures, the blast wave properties show little dependence on the ionization state of the debris ions. This is because the Al ions lose essentially all of their energy in a very small volume of gas near the target regardless of the free electron stopping cross-sections.

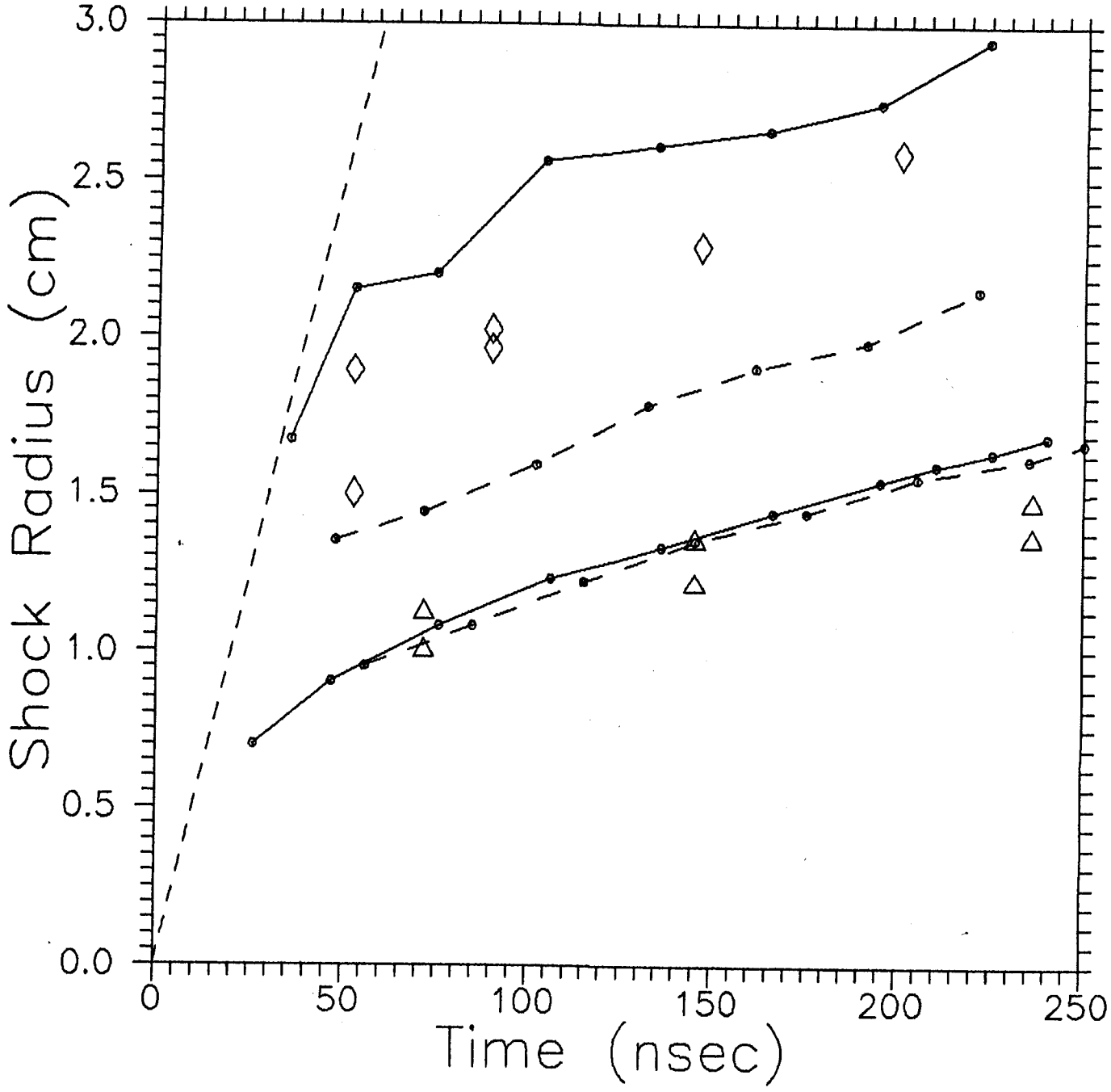

Fig. 6. Shock front radius vs. time. Calculated values are shown for Al^{4+} (solid curves) and Al^{2+} (dashed curves) for 0.1 torr (top curves) and 5.0 torr cases. Experimental data are shown for ambient gas pressures of 0.1 torr (diamonds) and 5.0 torr (triangles).

We have also performed calculations for a case with 0.025 torr background gas and found good agreement with the NRL data when the ionization state of the Al ions was increased to 6. The "average" charge state of the debris ions should of course increase as the background gas pressure decreases because the distance an Al ion must travel before capturing each electron becomes larger. Although the blast wave properties at this ambient pressure are extremely sensitive to the assumed ionization states of the Al ions, we have demonstrated that a model based on classical collision theory can quite adequately describe the energy transfer from the debris ions to the background gas in the NRL experiments. Collective effects, which are not included in our stopping cross-section model, are not required to increase the "effective" collisional interaction, and so are probably not a significant source of momentum transfer for ambient pressures down to 25 mtorr.

In another study, Kacenjar et al.[7] reported the results of computer simulations in which they calculated the hydrodynamic and magnetic properties resulting from spherical plasma expansions occurring in the presence of a magnetic field. In their simulations, rate equations for various collisional processes were used to calculate the evolution of the ionization states of the aluminum and nitrogen particles. In a problem similar to one reported in their paper, we calculated the response of a 0.2 torr background gas to an 82 J spherical expansion of Al ions. Whereas Kacenjar et al. found the shock front radius (defined by peak electron density) at 100 ns to be $\sim$ 1.0 cm, our calculations predict a substantially larger shock radius of 1.6 cm. Interestingly, by reducing the charge state of the Al ions in our calculations from 4 to 0 (i.e., neutral Al), the shock radius at 100 ns decreases to 1.0 cm. That is, the two calculations produce similar results when we completely neglect

the effects of collisions between the Al ions and free electrons in our calculations.

We can estimate what the observed shock radius at 100 ns was in the 0.2 torr NRL experiments from the "coupling efficiency" curves of Ripin et al.[4] From emission photography data, the shock radius is estimated to be 1.5 ± 0.1 cm. Although a smaller radius (1.1 ± 0.2 cm) is predicted from shadowgraphic measurements, the emission front results are expected to be more reliable when the background gas pressure is $\lesssim$ 0.3 torr.[6] Our simulations best reproduce the emission photography data when the charge state of the Al ions is ~ 3. Note that this ionization state also produced the best agreement with experimental data at 0.1 and 0.3 torr (see above).

Strong shock theory has been used[1,4] to find the "effective" energy coupled into the blast waves in the NRL experiments. But this approach is only valid when: 1) energy losses (e.g., due to radiation) are unimportant, and 2) at times and distances that are large compared to those over which the energy is deposited. Our calculations indicate that the second condition does not hold for the lower pressure experiments ($\lesssim$ 1 torr). Figure 7 shows the spatially integrated debris ion energy deposited as a function of distance from the target. The total ion kinetic energy used in these calculations was ~ 150 J, and results are shown for 4 different initial gas pressures. At 5 torr, it is seen that essentially all of the ion energy is deposited within ~ 0.5 cm from the target. At lower pressures, however, the volume over which the energy is deposited increases substantially. Only 50% of the energy from the Al ions has been transferred to the background within a radius of ~ 1.8 and 5.4 cm for the 0.3 and 0.1 torr cases, respectively. By comparison, the

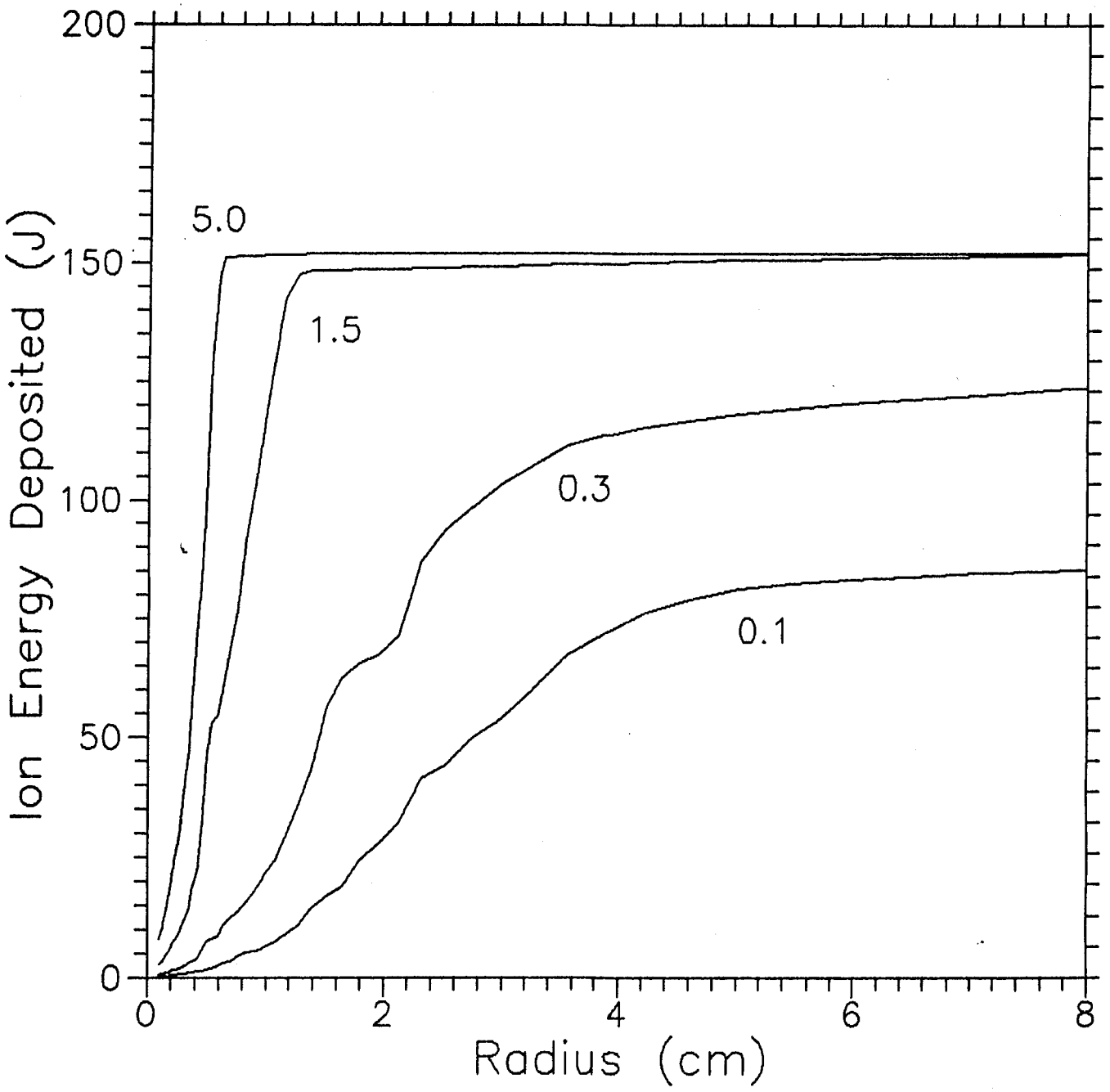

Fig. 7. Integrated Al ion energy deposition as a function of radius for calculations with an ambient gas pressure of 5.0, 1.5, 0.3, and 0.1 torr. Total Al ion kinetic energy in each calculation was 150 J.

maximum shock radii measured in the NRL experiments is ~ 2.5 cm. Hence, strong shock theory will not be as reliable when estimating the properties of blast waves in the NRL experiments for the pressures much below 1 torr.

Another reason the shock trajectories in Fig. 5 should not follow those predicted by strong shock theory ($r \propto t^{2/5}$) is that hydrodynamic motion is not the dominant means of energy transport at early times. This is more readily seen at the lower nitrogen gas pressures. (Although this effect is not clearly seen in the NRL data shown here, it is much more noticeable for the 0.025 and 0.044 torr data.[4,6]) At early times, the radius increases at a rate roughly equal to the debris ion velocity. At low ambient pressures, the Al ions transfer enough energy to heat the background gas, but not enough to significantly slow the ions. During this time, electron conduction is redistributing within the microfireball energy that was deposited by the debris ions. Eventually, the debris ions are stopped; in the case of low pressures, they are unable to heat the background gas sufficiently to cause significant ionization. The latter occurs because the flux of Al ions decreases as $1/r^2$ ($r \equiv$ distance from the target). When the debris ions are unable to sufficiently heat the gas to the point that electron thermal conduction is important, hydrodynamic flow becomes the primary means of energy transport. In our 0.1 torr calculation, the shock radius does not follow a $r \propto t^{2/5}$ trajectory until times $\gtrsim$ 200 ns.

The above results show that the stopping power model in CONRAD, which is based on classical collision theory, can explain the blast wave properties observed in the NRL experiments for ambient gas pressures down to 25 mtorr. The calculations best reproduce the experimental blast wave data in the 0.1 to 0.3 torr range when a charge state of 3 is assumed for the Al ions, and at

0.025 torr when a charge state of 6 is used. For background gas pressures $\gtrsim$ 1 torr, the shock radius is relatively insensitive to the assumed ionization state of the Al ions. The increase in the ionization state of the Al projectiles should be expected because the Al ions must travel farther before capturing an electron in a lower density plasma.

B) Radiation-Hydrodynamic Calculations

We next examine how including radiative transport in the energy equations affects the results of our simulations. We have performed a series of calculations similar to those described in Section III.A, but this time radiation transport is included using a flux-limited diffusion model.

Figures 8(a) through 8(d) show results from a radiation-hydrodynamic calculation assuming a total debris ion energy of 70 J and an ambient N_2 gas pressure of 5 torr. Plotted as a function of radius are the plasma temperature, radiation temperature, plasma pressure, and electron density. Comparing Fig. 8(a) with Fig. 4(a), it is seen that the plasma temperature is a factor of $\sim$ 4 to 6 lower when radiation transport is included in the calculation. The plasma temperature distribution is roughly isothermal at times $\gtrsim$ 100 ns. At earlier times, temperature variations persist because the plasma is emitting radiation faster than electron thermal conduction can reduce the gradients. This effect is not necessarily real, however, because the computed emission rate may be somewhat large due to our assumption that LTE exists. Figure 8(b) shows that the radiation temperature (defined to be proportional to the fourth root of the radiant energy density) is significantly lower than the plasma temperature, which indicates that the radiation field has not had time to equilibrate with the plasma. Instead, the relatively short diffusion

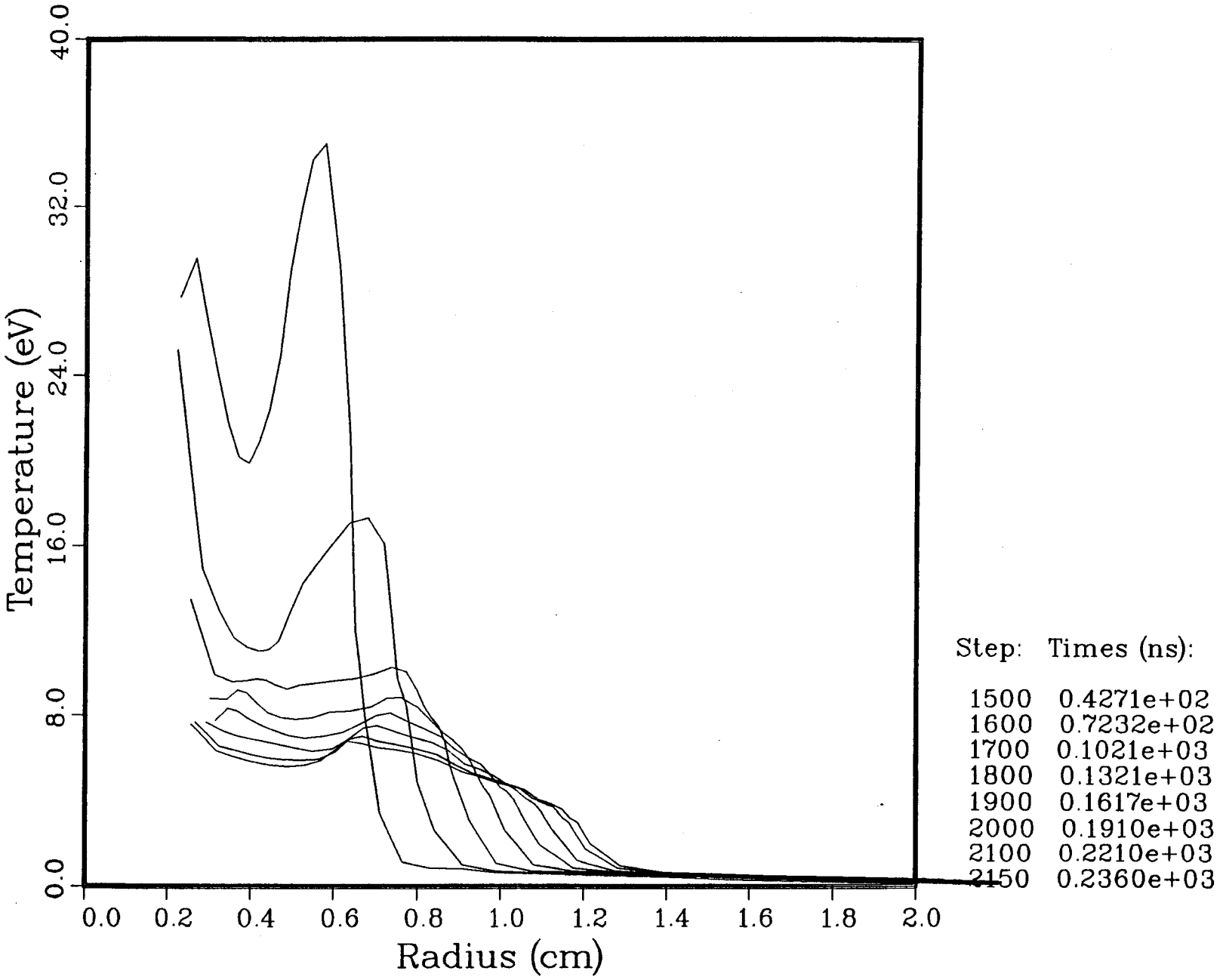

Fig. 8(a). Calculated plasma temperature as a function of radius at 8 different simulation times. Total Al kinetic energy was 70 J, and radiation effects were included.

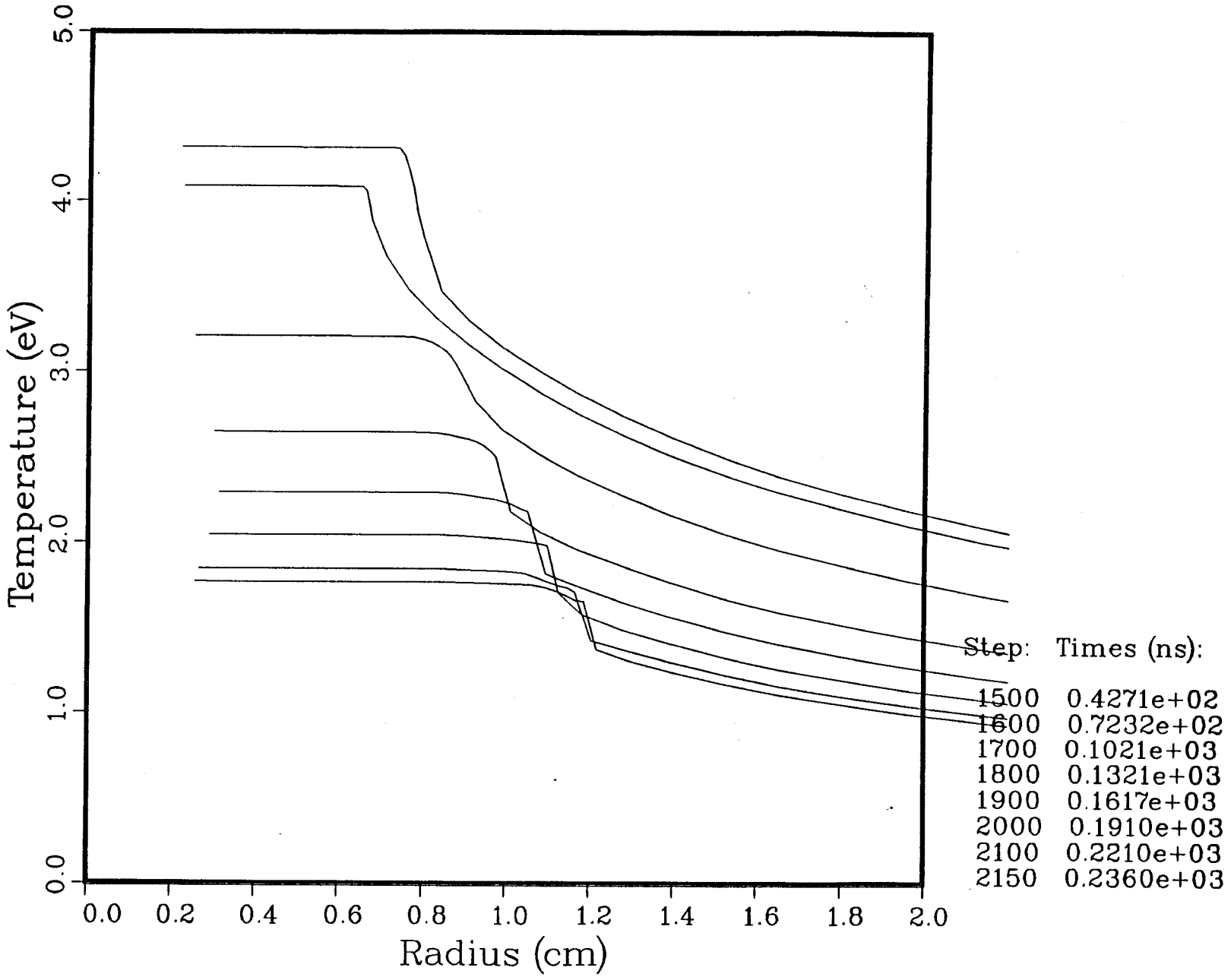

Fig. 8(b). Radiation temperature vs. radius (same calculation as Fig. 8(a)).

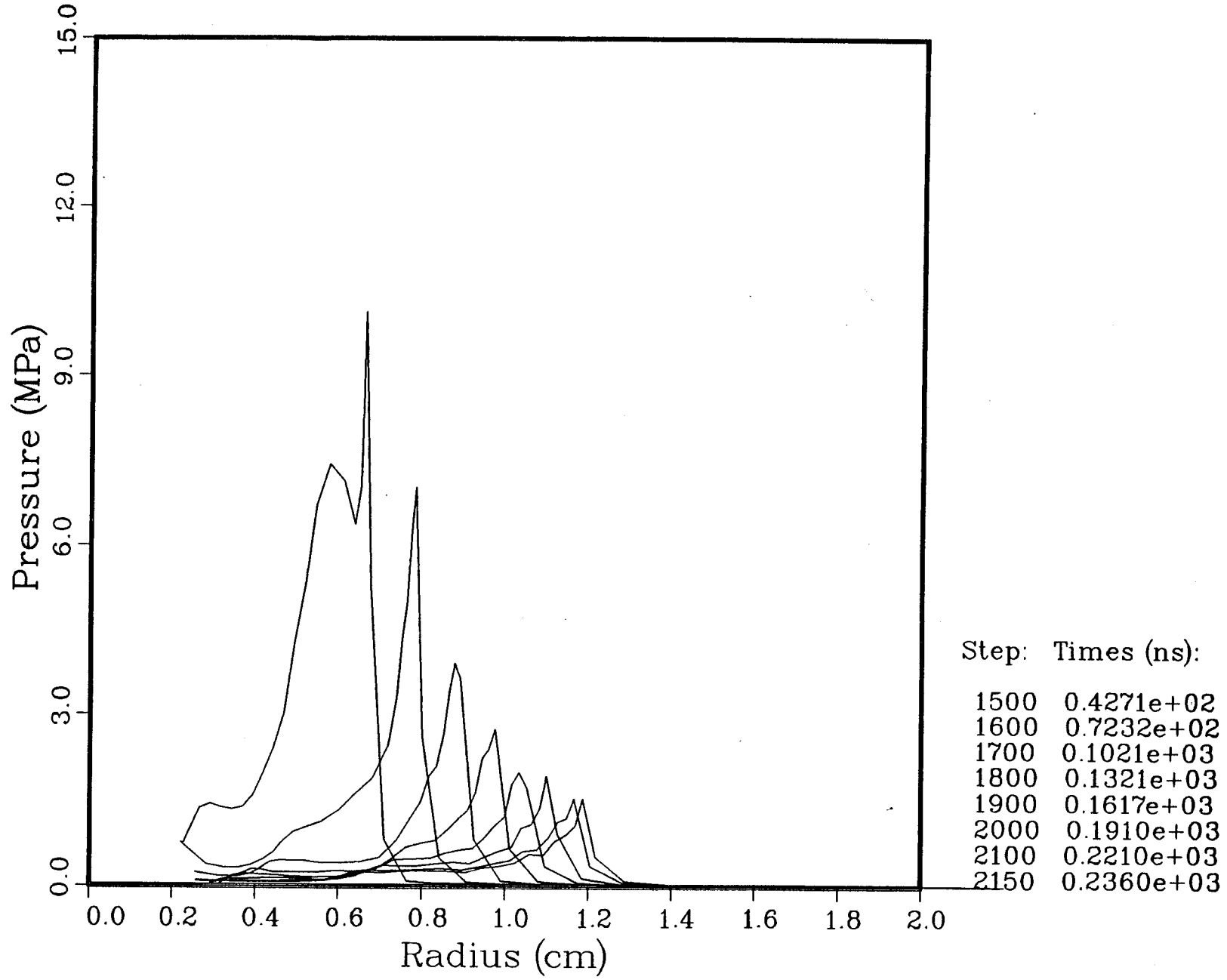

Fig. 8(c). Plasma pressure vs. radius (same calculation as Fig. 8(a)).

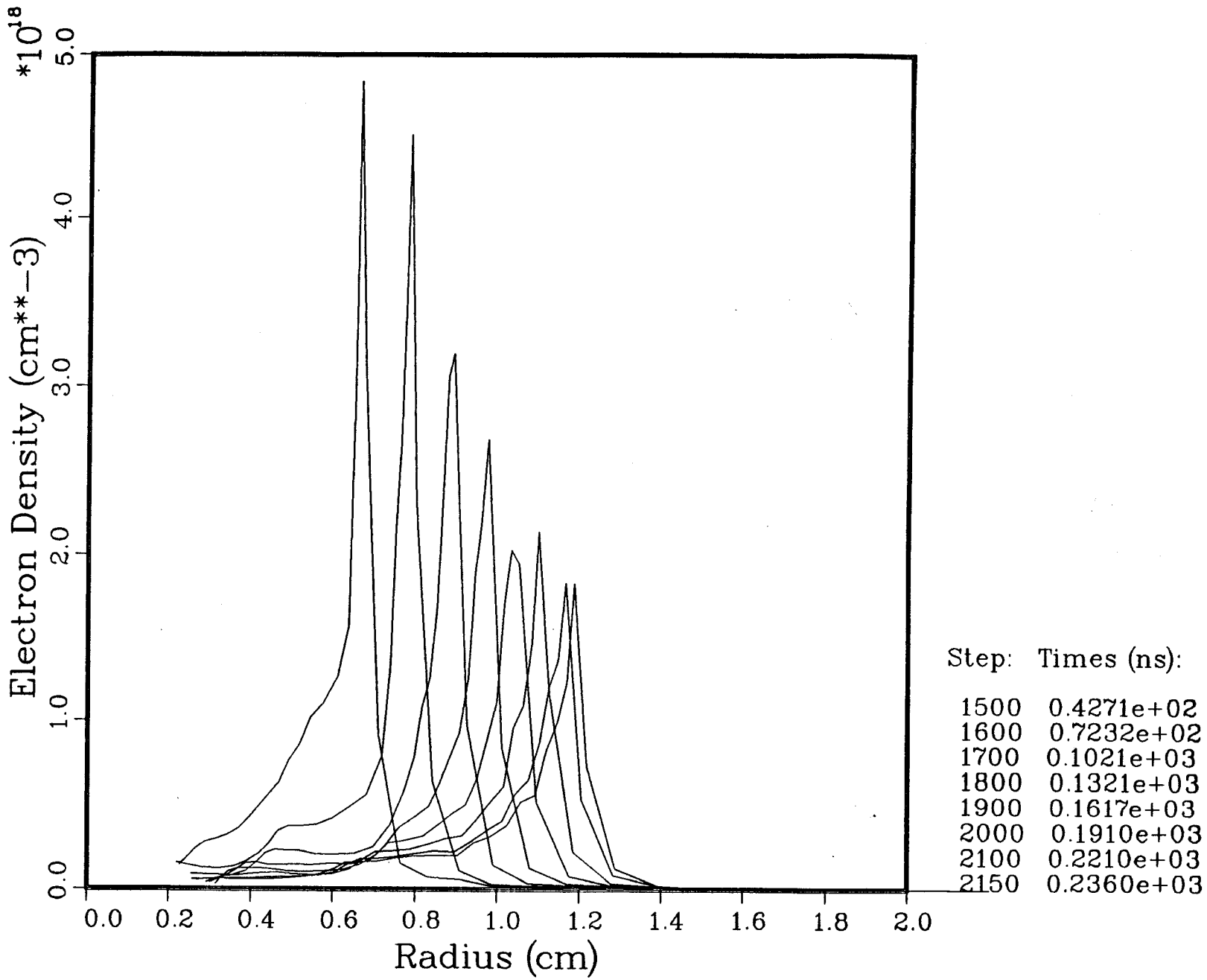

Fig. 8(d). Electron density vs. radius (same calculation as Fig. 8(a)).

times allow a significant fraction of the radiant energy to diffuse outward, far ahead of the shock front. Consequently, the escaping energy reduces the temperature in the microfireball, and less energy is available to generate hydrodynamic motion. This can result in a substantially weaker blast wave.

Because of the large radiation losses, the shock velocity is substantially lower. The shock arrival time at a distance of 1 cm from the target is 145 ns (Fig. 8(d)). This is roughly 50% longer than the value found from calculations in which radiation losses were ignored (Fig. 4(d)). In order to match the shock arrival time in the 25 J laser energy experiments of McLean et al. (see Section III.A), the total debris kinetic energy in our calculations must be raised to 140 J (i.e., a factor of 2 increase). Although the predicted electron density and temperature in the 140 J calculation are in agreement with the values derived from experimental data, it seems unlikely that such a large debris ion flux ($E_{ion}/E_{laser} \sim 5.6$) would be produced in the 25 J laser energy experiments.

Another interesting effect reported by McLean et al. was that a discrete jump in the continuum intensity was detected at a point 1 cm from the target roughly 50 ns before the shock front arrived.[3] The electron density in this "pre-step" region was estimated to be $\sim 2 \times 10^{18}$ cm^{-3}, or about 40% of the peak electron density observed when the shock front arrived. This effect is not observed in our calculations when the usual radiative transfer model was used (see Fig. 8(d)). But a "pre-step" was seen qualitatively in similar calculations in which the values in the opacity tables were increased by a factor of 100. Because of the shorter photon mean free paths, radiation emitted from behind the shock front can be reabsorbed in a region just ahead of the shock front instead of escaping to much farther distances. It seems

quite possible that given the uncertainties in the opacities, the "pre-step" observed in this experiment was caused by the absorption of radiation emitted from behind the shock front. This conclusion would also be consistent with the possibility that our opacities are somewhat low (see Section II.B).

The shock radii computed in a series of radiation-hydrodynamic calculations using a debris ion energy of 150 J are shown in Fig. 9. The initial background gas pressures range from 0.1 torr (top curve) to 5.0 torr. The open symbols again represent the NRL data. The calculated shock radii are somewhat larger that the experimental values for the 0.1 and 0.3 torr cases, but slightly small for the 1.5 and 5 torr cases. It is also seen that, except for the 5 torr case, the calculated shock velocities are somewhat lower than the experimental data predict. This indicates that too much energy is being radiated from behind the shock front in our calculations. When radiation losses are neglected, the calculated shock velocities are in much better agreement with the experimental data (see Fig. 5). Thus, as Ripin[11] has suggested, it appears that radiation plays a relatively minor role in the energy transport of the NRL experiments.

The large radiation losses in our calculations may arise from two problems. The first is that the values in our opacity tables are too low (see Section II.B). The second is that the radiation diffusion approximation is inappropriate to use for the conditions in these problems. The validity of the diffusion approximation can be tested by estimating the value of the photon mean free path. For a nitrogen gas at a temperature of $\sim$ 10 eV and a density corresponding to an initial pressure of 1 torr, the Rosseland opacity is $\sim 10^2$-10^3 $cm^2/gram$.[24] This leads to a photon mean free path of $\sim 10^2$-10^3

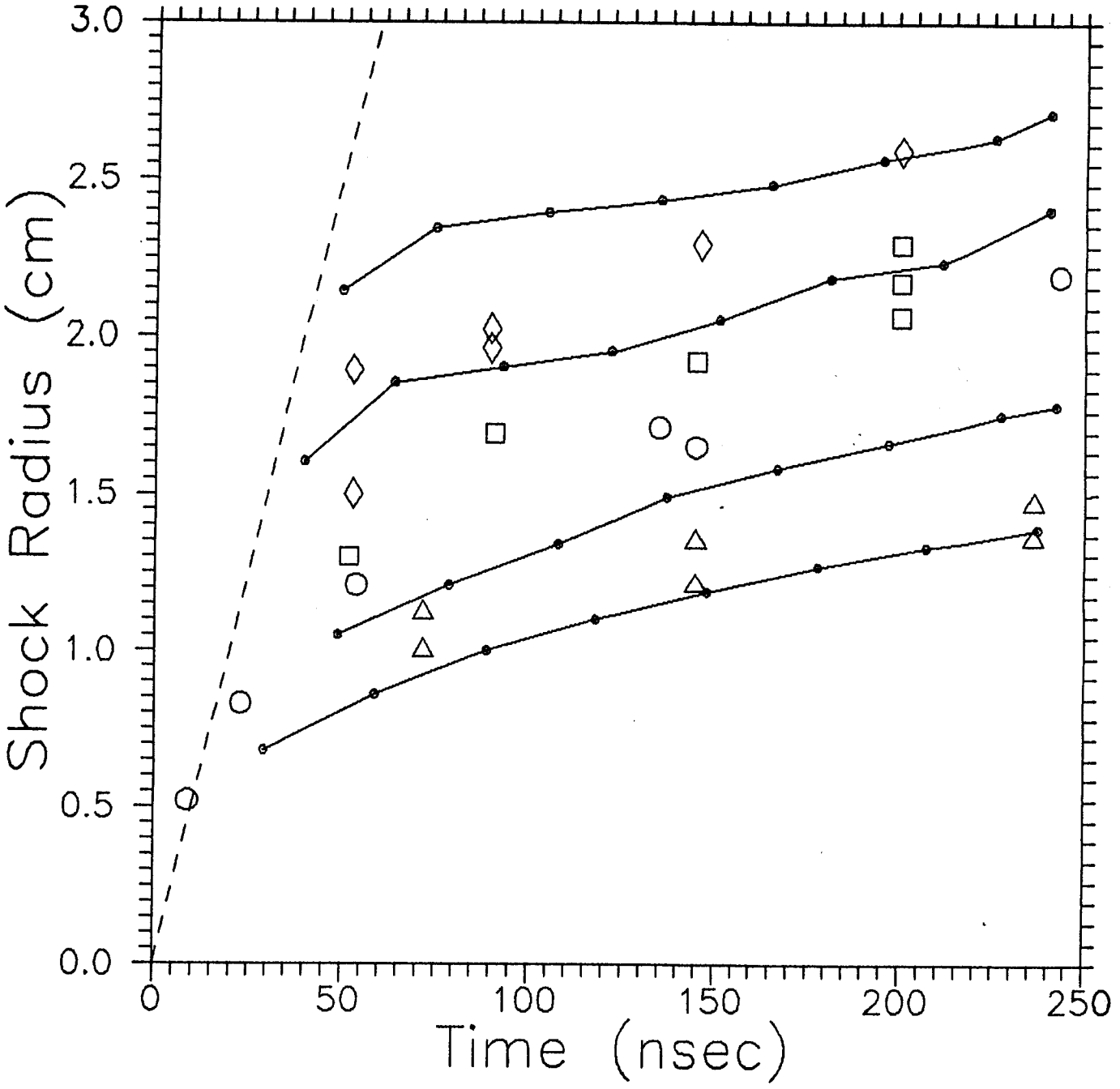

Fig. 9. Shock front radius vs. time. Solid curves represent calculated values. Radiation effects were included. Experimental data as shown for ambient gas pressures of 0.1 torr (diamonds), 0.3 torr (squares), 1.5 torr (circles), and 5.0 torr (triangles).

cm. Clearly, this violates the assumption that the photon mean free paths are small compared to the characteristic dimensions of the problem. Hence, the diffusion approximation may lead to rather inaccurate results in simulations of the NRL experiments.

IV. Conclusions and Discussion

The results we have presented indicate that the interactions between the expanding debris ions and the nitrogen background gas in the NRL experiments can be adequately modeled using classical collision theory. Collective effects are not required to explain the blast wave data down to pressures of at least 0.025 torr. We have also shown that the blast wave properties depend sensitively on the charge state of the debris ions for ambient gas pressures below 1 torr. This is because electron-ion collisions are the dominant mechanism of energy transfer from the debris ions in the experiments, and because the collisional mean free path becomes larger than the shock radius at the lower pressures.

The NRL blast wave data are best reproduced by calculations in which the initial debris ion kinetic energy is $\sim$ 150 J, the energy loss due to radiation is neglected, and the "average" charge state of the Al ions is $\sim$ 3 for ambient pressures of 0.1 to 0.3 torr and $\sim$ 6 for ambient pressures near 0.025 torr. The Al ions are expected to be more highly ionized in the lower density experiments because they must travel farther before capturing an electron. It is realized that computing the stopping cross-sections using a constant value for the Al charge state is rather simplistic. Although the charge state has been shown to be unimportant when the background gas pressure is $\gtrsim$ 1 torr,

calculations at lower pressures should include the effects of charge transfer between the debris ions and background plasma.

We suspect the rather large radiation losses in our calculations are caused by a breakdown in the assumptions of the radiation diffusion model and/or by opacity values that are too low. It is also expected that equilibrium assumptions used in our calculations are not always valid for the conditions that occur in the NRL experiments. For example, the mean collision time between electrons and ions is given by:[10]

$$\tau_{ei} \sim \frac{5 \times 10^7 \, A \, T_{ev}^{3/2}}{NZ^2}$$

where T_{ev} is the plasma temperature in eV, A is the atomic weight, Z is the charge state, and N is the ion number density. Thus, for A = 14 (nitrogen), T_{ev} = 10, Z = 2, and N = 7×10^{16} (corresponding to a gas pressure of 1 torr), the collision time is ~ 80 ns. Clearly, the equilibration time between the electron and ions is not small compared to the times discussed in this paper. This may be particularly important because the primary mechanism for transferring energy from the debris ions to the background plasma is ion-electron collisional interaction.

Finally, we mention that experiments such as those performed at NRL might be used to measure the stopping cross-sections of gases at high temperature. Measurements of the mass and average velocity of the debris ion reaching charge collection detectors have previously been made at various gas pressures. If reliable estimates of the electron density and charge states could be obtained, constraints could be placed on the stopping cross-sections for electron-ion collisions. Also, measurements of the debris ion charge

states at various distances from the target could provide valuable information about the charge transfer process.

Acknowledgment

This work was supported in part by the Lawrence Livermore National Laboratory. Computing support has been provided by the National Science Foundation at the San Diego Supercomputer Center.

References

1. B.H. Ripin, A.W. Ali, H.R. Griem, J. Grun, S.T. Kacenjar, C.K. Manka, E.A. McClean, A.N. Mostovych, S.P. Obenschain and J.A. Stamper, in Laser Interaction and Related Plasma Phenomena, Vol. 7, edited by G. Miley and H. Hora (Plenum, New York, 1986), pp. 857-877.

2. B.H. Ripin, J.A. Stamper and E.A. McClean, NRL Memorandum Report 5279, Naval Research Laboratory, Washington, D.C. (1984).

3. E.A. McClean, J.A. Stamper, H.R. Griem, A.W. Ali, B.H. Ripin and C.K. Manka, NRL Memorandum Report 5274, Naval Research Laboratory, Washington, D.C. (1984).

4. B.H. Ripin, E.A. McClean, J.A. Stamper, J. Grun, C.K. Manka and A.N. Mostovych, ETHANL, Issue #7, p. 75, SRI International, Menlo Park, CA (1987).

5. A.W. Ali and E.A. McClean, J. Quant. Spectrosc. Radiat. Transfer 33, 381 (1985).

6. E.A. McClean, B.H. Ripin, A.W. Ali, H.R. Griem, J. Grun, C.K. Manka, A.N. Mostovych, S.P. Obenschain and J.A. Stamper, ETHANL, Issue #7, p. 20, SRI International, Menlo Park, CA (1987).

7. S. Kacenjar, M. Hausman, M. Keskinen, A.W. Ali, J. Grun, C.K. Manka, E.A. McLean and B.H. Ripin, Phys. Fluids 29, 2077 (1986).

8. R.R. Peterson, G.A. Moses, R.L. Engelstad, D.L. Henderson, G.L. Kulcinski, E.G. Lovell, M.E. Sawan, I.N. Sviatoslavsky, J.J. Watrous, R. E. Olson and D.L. Cook, Fusion Tech. 8, 1895 (1985).

9. B. Badger, S.I. Abdel-Khalik, H.M. Attaya, R.L. Engelstad, G.L. Kulcinski, H.J. Liang, E.G. Lovell, G.A. Moses, Z. Musicki, R.R. Peterson, M.E. Sawan, I.N. Sviatoslavsky, L.J. Wittenberg, C. Verdon, R. McCrory, P. McKenty and S. Skupsky, UWFDM-711, Fusion Technology Institute, University of Wisconsin, Madison, WI (1986).

10. Y.B. Zel'dovich and Y.P. Raizer, Physics of Shock Waves and High-Temperature Hydrodynamic Phenomena (Academic Press, New York, 1966).

11. B.H. Ripin, private communication (1986).

12. R.R. Peterson, UWFDM-670, Fusion Technology Institute, University of Wisconsin, Madison, WI (1986).

13. G.A. Moses, R.R. Peterson and T.J. McCarville, Comput. Phys. Commun. 36, 249 (1985).

14. T.A. Melhorn, J. Appl. Phys. 52, 6522 (1981).

15. J. Lindhard and M. Scharff, Phys. Rev. 124, 128 (1961).

16. L.H. Thomas, Proc. Camb. Phil. Soc. 23, 542 (1927). E. Fermi, Z. Phys. 48, 73 (1930).

17. L.C. Northcliffe and R.F. Schilling, Nuc. Data Tables A7, 233 (1970).

18. J.J. Andersen and J.F. Ziegler, Hydrogen Stopping Powers and Ranges in All Elements (Pergamon, New York, 1977).

19. J.H. Ormrod, J.R. Macdonald and H.E. Duckworth, Can. J. Phys. 43, 275 (1965).

20. J.D. Jackson, Classical Electrodynamics, 2nd Edition (Wiley, New York, 1975).

21. R.R. Peterson and G.A. Moses, Comput. Phys. Commun. 28, 405 (1983).

22. D. Mihalas and B.W. Mihalas, Foundations of Radiation Hydrodynamics (Oxford, New York, 1984).

23. W.F. Huebner, A.L. Merts, N.H. Magee, Jr. and M.F. Argo, LA-6760-M, Los Alamos Scientific Laboratory, Los Alamos, NM (1977).

24. Opacity value calculated using MIXERG; see Ref. 21.

25. J. Grun, R. Decoste, B.H. Ripin and J. Gardner, Appl. Phys. Lett. 39, 545 (1981). J. Grun, R. Stellingwerf and B.H. Ripin, Phys. Fluids 29, 3390 (1986).